Efficient magnetic hysteresis model for field and stress application in magnetostrictive Galfenol

P. G. Evans and M. J. Dapino[a)]
Department of Mechanical Engineering, The Ohio State University, Columbus, Ohio 43210, USA

(Received 3 November 2009; accepted 18 January 2010; published online 29 March 2010)

We present a discrete energy-averaged model for the nonlinear and hysteretic relation of magnetization and strain to magnetic field and stress. Analytic expressions from energy minimization describe three-dimensional rotations of domains about easy crystal directions in regions where domain rotation is the dominant process and provide a means for direct calculation of magnetic anisotropy constants. The anhysteretic material behavior due to the combined effect of domain rotation and domain wall motion is described with an energy weighted average while the hysteretic material behavior is described with an evolution equation for the domain volume fractions. As a result of using a finite set of locally defined energy expressions rather than a single globally defined expression, the model is 100 times faster than previous energy weighting models and is accurate for materials with any magnetocrystalline anisotropy. The model is used to interpret magnetization and strain measurements of ⟨100⟩ oriented $Fe_{79.1}Ga_{20.9}$ and $Fe_{81.5}Ga_{18.5}$ as well as ⟨110⟩ oriented $Fe_{81.6}Ga_{18.4}$. © *2010 American Institute of Physics*. [doi:10.1063/1.3318494]

I. INTRODUCTION

Magnetostrictive materials deform when exposed to magnetic fields and undergo magnetization changes in response to stress. In these materials, the mechanical stiffness and magnetic permeability depend on both magnetic field and stress. Galfenol, an alloy of iron and gallium, is an emerging magnetostrictive material which exhibits a relatively high magnetomechanical coupling and mechanical properties similar to steel. This unique combination of properties enables unprecedented adaptive structures, sensors, and actuators with three-dimensional (3D) functionality and load-bearing capabilities. The effective design and control of Galfenol systems therefore requires advanced models capable of accurately describing 3D magnetomechanical behavior while simultaneously being computationally efficient.

In the work of Armstrong,[1] any bulk quantity related to magnetic moment orientation, such as magnetization or magnetostriction, is the expected value of a large collection of magnetic moments. The probability density function is the Boltzmann distribution in which all possible moment orientations are considered and minimum energy orientations are the most likely. While this model was formulated to describe anhysteretic Terfenol-D measurements, extensions include hysteresis in the presence of changing magnetic fields.[2] The hysteresis extension of the model lacks accuracy due to the choice of moment orientations included in the summation for the expected value calculations—only moments attaining a local internal energy minimum are included (eight for Terfenol-D and six for Galfenol.) Atulasimha *et al.*,[3] improved the accuracy of the hysteresis model by including 98 distributed orientations. The number of moments and their directions was chosen for ⟨110⟩-oriented material and may be different for other orientations. Evans and Dapino[4] described rate dependent hysteresis in magnetization and magnetostriction by tracking the transitions of a large collection of moments between energy wells. They then reverted to a reduced number of possible orientations but used the local minima of the free energy, which includes magnetic and magnetomechanical work terms.[5] This approach was shown to simultaneously achieve the accuracy and computational speed required for device characterization, design, and control.

These energy-weighted models have three critical limitations. The first is that the form of the magnetocrystalline anisotropy energy, which determines the orientations preferred by magnetic moments, is material specific. Current material processes for Galfenol are capable of significantly changing the magnetocrystalline anisotropy energy,[6] hence determination of the appropriate form of the anisotropy energy can be challenging and difficult to generalize. The second limitation of previous models is the absence of a mechanism for magnetic hysteresis under stress application, which is critical for design of sensors and actuators exposed to variable mechanical loads. The third limitation is that minor loops from field application have negative susceptibility at the field reversal points, which is inconsistent with data. These limitations are addressed in this paper.

First, a general formulation for magnetocrystalline anisotropy energy is developed. Rather than seek to define a global energy which includes the local energy minima or preferred orientations, we define the anisotropy energy locally about the known preferred orientations. The total free energy with locally defined anisotropy is minimized to calculate the orientation of domains. Second, the magnetic hysteresis model is extended to account for hysteresis resulting from both magnetic field and stress application. A single parameter characterizes the hysteresis delay in both cases. Third, we include the effect of reversible changes in domain

[a)]Author to whom correspondence should be addressed. Electronic addresses: dapino.1@osu.edu and evans.895@osu.edu.

walls from wall bowing, while restricting the effect of irreversible processes so as to exclude the unphysical behavior of negative susceptibility.

II. MODEL DEVELOPMENT AND EXPERIMENTS

Ferromagnetic materials are composed of regions of uniform magnetization M_s called domains.[7] In the Stoner–Wohlfarth (SW) approximation used here and in other magnetomechanical models,[8] the material is modeled as a collection of noninteracting, single-domain particles.[9] The internal energy of a particle is due to magnetocrystalline anisotropy which gives domains preferred or easy directions. Work is required to rotate domains away from the easy directions. As magnetic fields $\mathbf{H}$ and stresses $\mathbf{T}$ are applied, domains rotate towards the field direction and perpendicular to the principal stress directions. When magnetic domains rotate, the magnetomechanical coupling induces lattice strain and bulk magnetostriction. For a material composed of a collection of SW particles in thermodynamic equilibrium having r possible orientations, the bulk magnetization $\mathbf{M}$ and magnetostriction $\mathbf{S}_m$ are the sum of the magnetization $M_s\mathbf{m}^k$ and magnetostriction $\mathbf{S}_m^k$ due to each orientation, weighted by the volume fraction ξ^k of particles in each orientation

$$\mathbf{M} = M_s \sum_{k=1}^{r} \xi^k \mathbf{m}^k, \quad \mathbf{S}_m = \sum_{k=1}^{r} \xi^k \mathbf{S}_m^k. \tag{1}$$

The total strain is the sum of the magnetostriction and the purely mechanical strain $\mathbf{sT}$, where $\mathbf{s}$ is compliance. The anhysteretic values of the volume fractions are calculated using an energy-weighted average,

$$\xi_{an}^k = \frac{\exp(-G^k/\Omega)}{\Sigma_{k=1}^{r} \exp(-G^k/\Omega)}. \tag{2}$$

The energy G^k is the part of the free energy related to orientation $\mathbf{m}^k$ and parameter Ω is the Armstrong smoothing factor. A Boltzmann-type, energy weighting expression was first proposed for use in magnetostrictive materials by Armstrong[1,2] and applied to Galfenol by Atulasimha *et al.*[10] The cited works use a large number r of fixed directions $\mathbf{m}^k$. Evans and Dapino[5] reduced r while maintaining accuracy by utilizing only $\mathbf{m}^k$ which attain a local energy minimum.

A. Energy formulation

The free energy of a magnetostrictive material has terms for magnetic anisotropy, magnetomechanical coupling, and Zeeman or field energy. These energies are formulated by idealizing the complex domain structure of ferromagnetic materials as a system of noninteracting, single-domain, SW particles. The system of SW particles is composed of r distinct groups or variants which rotate about an energetically favorable or easy direction which for the k^{th} variant is $\mathbf{c}^k$. The variants are distinguished by their easy directions. The free energy is formulated separately for each of the variants whereas in previous work (Atulasimha *et al.*,[3] and Evans and Dapino[5]) a single energy expression is used for any SW particle orientation. The benefit of this approach is that the anisotropy energy depends explicitly on the variant's easy direction. We can thus describe arbitrary anisotropy symmetries, needing only a knowledge of the easy directions.

The anisotropy energy of the k^{th} variant, G_A^k, is the work required to rotate a SW particle away from $\mathbf{c}^k$. This is analogous to mechanical systems where work is required to displace a spring from equilibrium. This can be expressed as

$$G_A^k = \frac{1}{2} K^k |\mathbf{m}^k - \mathbf{c}^k|^2. \tag{3}$$

For materials with a cubic lattice, the ⟨100⟩ or ⟨111⟩ directions tend to be easy. The anisotropy coefficient in each direction family is the same, thus $K^k = K_{100}$ for all six ⟨100⟩ directions and $K^k = K_{111}$ for all eight ⟨111⟩ directions. For negative anisotropy coefficients K^k, the direction $\mathbf{c}^k$ is magnetically hard or an unstable equilibrium. Galfenol can thus have 6, 8, or 14 easy directions, which dictates the number of variants r. While unannealed Galfenol is generally cubic and thus has either one or two distinct K^k coefficients, stress annealing or residual stresses from the crystal growth process can cause a change in symmetry resulting in distinct values for K^k within the orientation families ⟨100⟩ and ⟨111⟩.

The magnetomechanical coupling energy G_C^k of a single SW particle with magnetization M_s is the strain energy density resulting from the magnetostriction of the particle,

$$G_C^k = -\mathbf{S}_m^k \cdot \mathbf{T}, \tag{4}$$

and the Zeeman energy is

$$G_Z^k = -\mu_0 M_s \mathbf{m}^k \cdot \mathbf{H} \tag{5}$$

Kittel[7] provides expressions for the magnetostriction of a SW particle with cubic symmetry

$$\mathbf{S}_m^k = \begin{bmatrix} (3/2)\lambda_{100}(m_1^k)^2 \\ (3/2)\lambda_{100}(m_2^k)^2 \\ (3/2)\lambda_{100}(m_3^k)^2 \\ 3\lambda_{111} m_1^k m_2^k \\ 3\lambda_{111} m_2^k m_3^k \\ 3\lambda_{111} m_3^k m_1^k \end{bmatrix}. \tag{6}$$

The total free energy for each particle variant therefore is

$$G^k = \frac{1}{2} K^k |\mathbf{m}^k - \mathbf{c}^k|^2 - \mathbf{S}_m^k \cdot \mathbf{T} - \mu_0 M_s \mathbf{m}^k \cdot \mathbf{H}, \tag{7}$$

which is minimized to calculate the particle orientation.

1. Calculation of particle orientations

The magnetic orientations $\mathbf{m}^k$ of the SW particles are calculated from minimization of Eq. (7) with constraint $C = |\mathbf{m}^k| - 1 = 0$ (since $\mathbf{m}^k$ is a unit vector). The constrained minimization can be formulated as an inhomogeneous eigenvalue problem through the use of Lagrange multipliers. Gathering terms from Eq. (7) and expressing the particle free energy as $G^k = \frac{1}{2}\mathbf{m}^k \cdot \mathbf{K}^k \mathbf{m}^k - \mathbf{m}^k \cdot \mathbf{B}^k$, one can write the eigenvalue problem as

$$(\mathbf{K}^k - \gamma \mathbf{I})\mathbf{m}^k = \mathbf{B}^k, \tag{8}$$

where the magnetic stiffness matrix $\mathbf{K}^k$ and force vector $\mathbf{B}^k$ are

$$\mathbf{K}^k = \begin{bmatrix} K^k - 3\lambda_{100}T_1 & -3\lambda_{111}T_4 & -3\lambda_{111}T_6 \\ -3\lambda_{111}T_4 & K^k - 3\lambda_{100}T_2 & -3\lambda_{111}T_5 \\ -3\lambda_{111}T_6 & -3\lambda_{111}T_5 & K^k - 3\lambda_{100}T_3 \end{bmatrix}, \tag{9}$$

$$\mathbf{B}^k = \begin{bmatrix} c_1^k K^k + \mu_0 M_s H_1 & c_2^k K^k + \mu_0 M_s H_2 & c_3^k K^k + \mu_0 M_s H_2 \end{bmatrix}^T. \tag{10}$$

While the orientations can be easily solved for in terms of γ, determination of γ requires solution of a sixth-order polynomial obtained by substitution of each γ-dependent orientation into the constraint. The constraint is relaxed through linearization about the easy direction $\mathbf{c}^k$. This has little effect on the calculated bulk magnetization and magnetostriction, since the energy weighting operation [Eq. (1)] ensures that particles which have rotated far from the easy axis are less likely or have smaller volume fractions than those particles which have not rotated far. In other words, the orientations which have easy axis near the field direction and perpendicular to the stress direction are most favorable. For the linearized constraint, the solution to the inhomogeneous eigenvalue problem is

$$\mathbf{m}^k = (\mathbf{K}^k)^{-1}\left[\mathbf{B}^k + \frac{1 - \mathbf{c}^k \cdot (\mathbf{K}^k)^{-1}\mathbf{B}^k}{\mathbf{c}^k \cdot (\mathbf{K}^k)^{-1}\mathbf{c}^k}\mathbf{c}^k\right]. \tag{11}$$

The particle orientations [Eq. (11)] define the orientations to be included in the energy averaging [Eq. (1)], thus in the present formulation r depends on the number of easy axes. Galfenol has six easy axes in the ⟨100⟩ directions.

2. Comparison between the Armstrong model for cubic materials and the discrete energy-averaged model

The traditional manner of expressing anisotropy energy is to define a global energy expression as a function of SW particle orientation, which has minima corresponding to the easy axes. The form for cubic materials is[7,11]

$$G_A = K_4(m_1^2 m_2^2 + m_2^2 m_3^2 + m_3^2 m_1^2). \tag{12}$$

The subscript of the anisotropy coefficient refers to the order of the expression which is fourth-order in this case. This energy has extrema in the ⟨100⟩ and ⟨111⟩ directions, consistent with Galfenol, and for this reason it has been used in magnetomechanical models for Galfenol.[3,5] The anisotropy of Galfenol can be changed through stress annealing (application of stress at elevated temperatures.) Annealing along a ⟨100⟩ direction has been shown to result in Galfenol material with tetragonal anisotropy where the four ⟨100⟩ directions perpendicular to the annealing direction have a lower energy than the remaining two.

The formulation by Trémolet[12] for tetragonal symmetry is

$$G_A = K_2\left(m_3^2 - \frac{1}{3}\right) + K_4\left(m_1^4 + m_2^4 + m_3^4 - \frac{3}{5}\right) + K_4'\left(m_3^4 - \frac{6}{7}m_3^2 + \frac{3}{35}\right), \tag{13}$$

where the [001] and [00$\bar{1}$] directions have different energies than the remaining four ⟨100⟩ orientations. The following reduced form for tetragonal symmetry has been used for stress-annealed Galfenol[4,6]

$$G_A = K_4(m_1^4 + m_2^4 + m_3^4) + K_2 m_3^2. \tag{14}$$

While for the global formulations different material symmetries necessitate different forms for G_A, adapting the locally defined expression [Eq. (3)] for different material symmetries requires only an adjustment of the coefficients. Another advantage of the local formulation is the simplicity of the minimization process. Consider for example a cubic material; the globally defined free energy G in this case is

$$G = K_4(m_1^2 m_2^2 + m_2^2 m_3^2 + m_3^2 m_1^2) - \mathbf{S}_m(\mathbf{m}) \cdot \mathbf{T} - \mu_0 M_s \mathbf{m} \cdot \mathbf{H}. \tag{15}$$

Depending on the values of the coefficients and the applied stress and field, this expression can have anywhere from one to six minima requiring a robust, nonlinear minimization scheme. The fact that minima can disappear presents a challenge when utilizing [Eq. (1)] to calculate the bulk magnetization and magnetostriction with direct energy minimization, since r varies with stress and field. To obviate this issue, previous works[5,13] considered small particle rotations by performing a second-order expansion of [Eq. (15)] about the easy crystal directions. The approach here is to formulate second-order energy expressions directly, for each easy direction.

A comparative study shows that minimum energy orientations using the globally defined energy are similar to the minimum orientations of the locally defined energies. Consider a material with cubic symmetry having ⟨100⟩ easy directions. For the global energy expression, Eq. (15) is used, and for the local formulation six expressions are used, one for each of the easy directions. Since the symmetry is cubic, all of the local expressions [Eq. (3)] have the same coefficient $K^k = K_{100}$ and differ only in $\mathbf{c}^k$.

When applying fields and stresses along the [100] direction, energy [Eq. (15)] initially has six minimum orientations. Two of the minima are

$$\mathbf{m} = \begin{bmatrix} \pm 1 \\ 0 \\ 0 \end{bmatrix}, \tag{16}$$

and the remaining four depend on stress and field, corresponding to the rotation of particles away from the four remaining ⟨100⟩ directions and towards the applied field. Stress tends to impede these rotations since it favors perpendicular directions. Evans[13] showed that for small rotations these minima have the following component in the [100] direction:

$$m_1 = \frac{\mu_0 M_s}{2K_4 - 3\lambda_{100}T} H. \tag{17}$$

The other components are simply zero or ±1.

The local energies [Eq. (7)] result in similar expressions for the six minima. For the energy expressions with $\mathbf{c}^k = [\pm 100]$ the minima are

$$\mathbf{m} = \begin{bmatrix} \pm 1 \\ 0 \\ 0 \end{bmatrix}, \tag{18}$$

and for the expressions with $\mathbf{c}^k = [0 \pm 10]$ and $\mathbf{c}^k = [00 \pm 1]$, the component in the [100] direction is

$$m_1 = \frac{\mu_0 M_s}{K_{100} - 3\lambda_{100}T} H, \tag{19}$$

and the other components are again zero or ±1. Since Eq. (17) and (19) describe the same magnetization process, $K_{100} = 2K_4$ should be satisfied.

The Armstrong model uses the global energy expression with fixed orientations whereas the discrete energy-averaged model presented here uses local energy expressions with field and stress dependent orientations. Calculation of bulk behavior using the two approaches yields similar results so long as one recognizes that $K_{100} = 2K_4$. Two cases are considered, [100] field application and [110] field application, both with a bias stress. The bulk magnetization is calculated using Eq. (2) with various values of smoothing parameter Ω. In the Armstrong model,[1] the global energy expression is used and r in Eq. (2) is a number of fixed particle orientations. In the model presented here, local energy expressions are used. For cubic symmetry, direct minimization of the energy corresponding to each variant yields $r=6$ orientations which rotate with stress and field application. To determine r in the Armstrong formulation, the discrete form [Eq. (2)] is found through discretization of the continuous form,

$$\xi(\phi, \theta) = \frac{\exp(-G/\Omega)\sin\phi d\phi d\theta}{\int_0^{\pi}\int_0^{2\pi}\exp(-G/\Omega)\sin\phi d\phi d\theta}, \tag{20}$$

where ξ is now interpreted as a probability density and the pair (ϕ, θ) represents the particle orientation in spherical coordinates. To numerically integrate, the integration intervals are discretized into N_I segments and over each segment, fourth-order Gauss quadrature is used. This results in $4N_I$ values each for ϕ and θ and $r = 16N_I^2$ total particle orientations. The required N_I for good accuracy depends on Ω. As

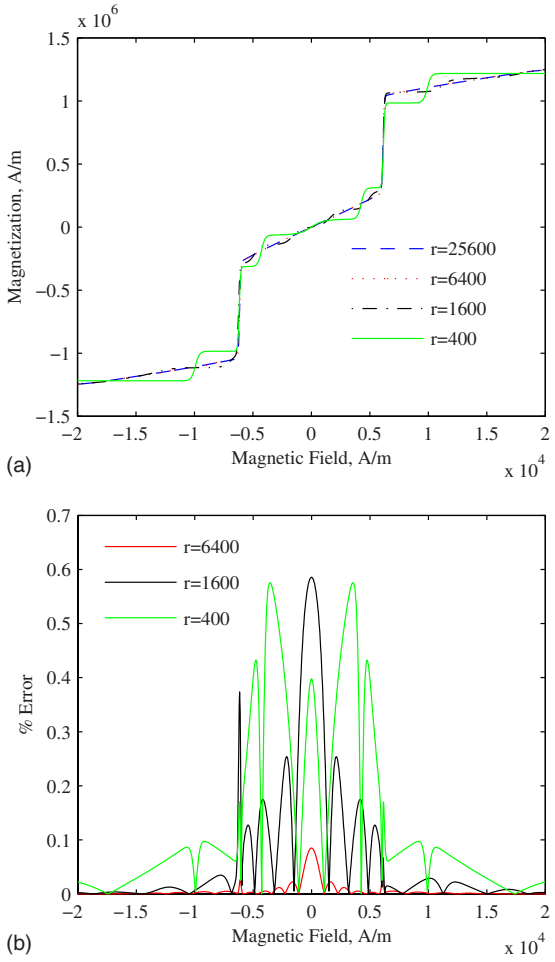

FIG. 1. (Color online) Effect of discretization in the Armstrong model. (a) Magnetization versus field at constant stress, where the field and stress are applied in the ⟨100⟩ direction. (b) Error relative to the $N_I=40$ ($r=25600$) case.

Ω approaches zero, $\xi=1$ for the globally minimum orientation and $\xi=0$ for all other orientations. In the Armstrong model, if the discretization is too coarse, then it may be that none of the fixed orientations are near the global minimum. In the model presented here, this issue does not arise because the global minimum is simply the minimum of the local minima, which are calculated explicitly. Figure 1(a) shows $M-H$ curves calculated with the Armstrong model at constant T in which H and T are applied in the ⟨110⟩ direction and Ω is low. Different values of N_I are used. Curves calculated with $N_I=20$ ($r=6400$) and $N_I=40$ ($r=25\,600$) show a small difference, therefore the error in the $N_I=40$ case is assumed negligible and this curve is taken as the benchmark for error calculations. The relative error was calculated for each of the curves at all field values and is shown in Fig. 1(b). The maximum error is less than 60% for $N_I=5$ and less than 10% for $N_I=20$.

Since it has been demonstrated that $r=25\,600$ results in good accuracy, this is used for Armstrong model calculations in comparing $M-H$ curves with the anhysteretic discrete energy-averaged model (see Fig. 2.) The anhysteretic discrete energy-averaged model uses the local energy definition [Eq. (7)], SW particle orientations [Eq. (11)], and discrete energy-average [Eq. (2)]. The model parameters used for the

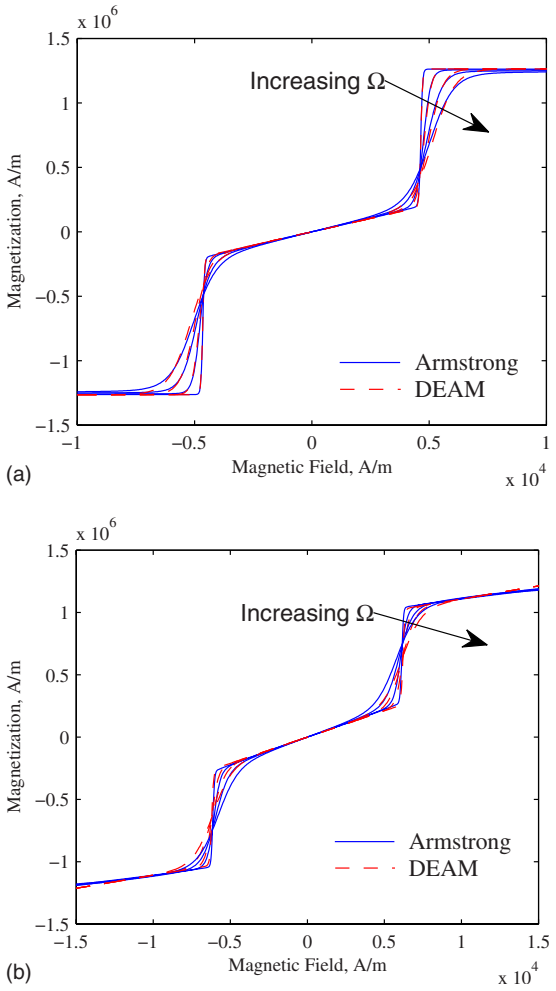

FIG. 2. (Color online) Comparison of the Armstrong model with the discrete energy-averaged model (DEAM) for Ω ranging from 50 to 600. (a) ⟨100⟩ calculations. (b) ⟨111⟩ calculations.

comparison in Fig. 2 are $\mu_0 M_s = 1.59$ T, $K_{100} = 2K_4 = 17.5$ kJ/m^3, $(3/2)\lambda_{100} = 260 \times 10^{-6}$, and $3\lambda_{111} = -10 \times 10^{-6}$ at various values of Ω (50, 100, 200, 400, and 600 J). A bias stress of −26 MPa is used for the ⟨100⟩ calculations and −50 MPa for the ⟨111⟩ calculations.

Although the difference between the Armstrong model and the model presented here is greater with increasing Ω, both models provide the same trends. When Ω is small, the magnetization is only due to the global minimum orientation. In this case the two models are nearly identical. There is a small difference at high fields (~10.5 kA/m) for ⟨110⟩ application owing to the fact that a linear approximation was used for computing the minimum of the local energy expressions for the discrete energy-averaged model. Though this error is small in all cases, it is greater when field or stress rotates particles to a direction far from the easy axes. In both models, an increasing Ω results in smoother curves. Whereas the curves for small Ω have sharp transitions representing a change in the global minimum from one local minimum to another, for large Ω the volume fractions or probability density are more broadly distributed, meaning that the bulk magnetization has contributions from the global minimum as well as the other local minima in the discrete energy-averaged model, and it has contributions from all the fixed orientations in the Armstrong model. The difference between the two models for higher Ω can be attributed to the presence of orientations that are neither global nor local minima in the Armstrong model, since the orientations used in the summation of the Armstrong model are found from Gauss-quadrature rules without regard to energy.

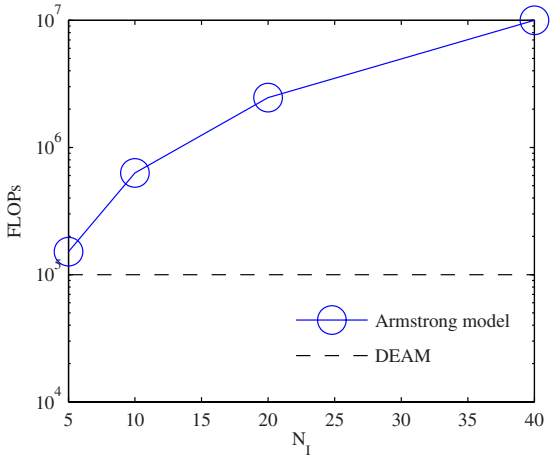

FIG. 3. (Color online) Number of floating-point operations required for the Armstrong model and the discrete energy-averaged model (DEAM).

The discrete energy-averaged model is computationally efficient since it utilizes only six particle orientations (see Fig. 3.) For the benchmark $N_I = 40$, the number of floating-point operations is 10×10^6. For the discrete energy-averaged model the number of orientations is fixed and the required number of floating-point operations is 0.1×10^6, an improvement of two orders of magnitude. This improvement is significant for device design and control.

3. ⟨100⟩ single-crystal $Fe_{79.1}Ga_{20.9}$ measurements and anhysteretic model

Magnetization versus magnetic field measurements at constant stress for [100]-oriented, single-crystal $Fe_{79.1}Ga_{20.9}$ are compared with the anhysteretic discrete energy-averaged model [Eqs. (2), (7), and (11)]. The material was grown with the Bridgman method resulting in a single-crystal rod. Although the material is body centered cubic, the magnetostriction measurements indicate that the magnetic anisotropy has tetragonal symmetry. Material with cubic symmetry has a maximum magnetostriction of λ_{100} in the [100] direction when no stress is applied and $(3/2)\lambda_{100}$ when sufficient stress is applied to align all domains perpendicular to the field and stress. The measurements in Fig. 4(b) show that the maximum magnetostriction exhibits little dependence on the bias stress. This suggests that the material has tetragonal symmetry where perpendicular domain orientations are energetically preferred to parallel domain orientations, even when no stress is applied. This could be due to either the crystal growth process or tetragonal material phases. Studies have shown that Fe–Ga alloys have a complicated phase diagram and any given alloy may have multiple phases present.[14]

The magnetization data has three linear regions separated by nonlinear transitions [see Fig. 4(a)]. In the model,

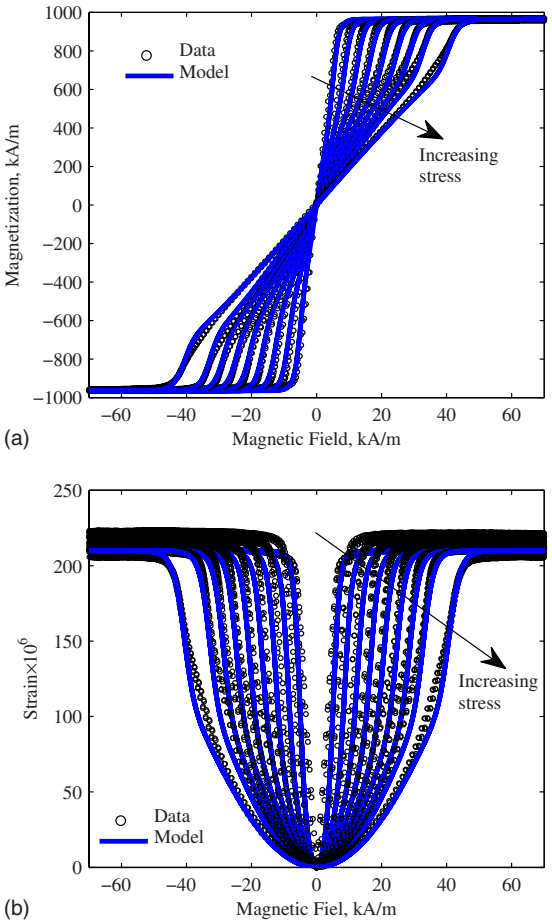

FIG. 4. (Color online) (a) Magnetization and (b) magnetostriction of ⟨100⟩ single-crystal $Fe_{79.1}Ga_{20.9}$ at constant stress values of 0.689, 13.8, 27.6, 41.3, 55.1, 68.9, 82.7, 96.4, and 123 MPa (compression), compared with anhysteretic model calculations.

these regions are described by three variants of SW particles. The linear region below the approach to magnetic saturation is dominated by rotation of particles away from the [010], $[0\bar{1}0]$, [001], and $[00\bar{1}]$ directions—orientations initially perpendicular to the applied stress and field—and into the field direction. These orientations have anisotropy coefficient $K_\perp$. The component of the orientation in the [100] direction, $m_\perp$ given by Eq. (19), results in a contribution of $M_\perp = M_s m_\perp(\xi_{010}+\xi_{0\bar{1}0}+\xi_{001}+\xi_{00\bar{1}})$ to the total magnetization. The remaining regions are the positive and negative magnetic saturation regions, where little magnetization change occurs with varying magnetic fields. These regions are dominated by [100] and $[\bar{1}00]$ particles which are already aligned with the field and stress axis. These particles have anisotropy coefficient $K_\parallel$. The former orientation contributes to positive saturation and the latter to negative saturation. Their contributions to the total magnetization are $M_{[100],[\bar{1}00]}=M_s\xi_{[100]}$, $-M_s\xi_{[\bar{1}00]}$.

The volume fractions are determined from the energy-weighted average [Eq. (2)]. Stresses favor the off-axis or initially perpendicular variants, each of which have the same energy level, from Eq. (7)

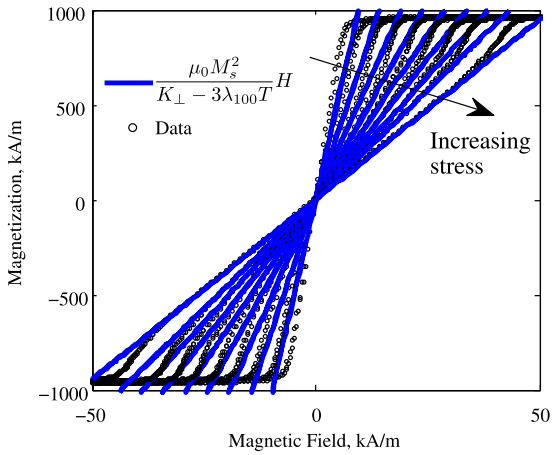

FIG. 5. (Color online) Rotation of perpendicular domain orientations compared with data of ⟨100⟩ single-crystal $Fe_{79.1}Ga_{20.9}$ at constant stress values of 0.689, 13.8, 27.6, 41.3, 55.1, 68.9, 82.7, 96.4, and 123 MPa (compression).

$$E_\perp = \frac{H^2(\mu_0 M_s)^2 - 3\lambda_{100}K_\perp T + K_\perp^2}{6\lambda_{100}T - 2K_\perp}. \tag{21}$$

Applied magnetic fields favor the parallel orientations which have energies

$$E_{[100],[\bar{1}00]} = \mp H\mu_0 M_s - \frac{3}{2}\lambda_{100}T - \frac{1}{2}K_\parallel. \tag{22}$$

With no applied field and stress, $E_\perp$ is much greater than $E_{[100],[\bar{1}00]}$. In the energy-weighted average this results in $\xi_{010}+\xi_{0\bar{1}0}+\xi_{001}+\xi_{00\bar{1}}\approx 1$ and the magnetization is simply Eq. (19); this expression is compared with the data in Fig. 5. The anisotropy constant $K_\perp$ can thus be calculated directly from the slope of the linear magnetization region. The kink in the magnetization curves or the transition from the linear region to saturation occurs when $E_\perp = E_\parallel$. This gives a measure of the other anisotropy coefficient $K_\parallel$. Two of the remaining parameters are determined directly from the data; M_s and $(3/2)\lambda_{100}$ are found from the magnetization and magnetostriction at saturation. The smoothing parameter Ω is determined through least-squares optimization and determines the sharpness of the transition to saturation. For ⟨100⟩ application, the shear magnetostriction coefficient λ_{111} does not enter into the model and hence cannot be determined from the data. The total magnetization as calculated by Eq. (2) is compared with the data in Fig. 4. The model parameters used for these calculations are provided in Table I.

B. Magnetomechanical hysteresis

Hysteresis is included in energy weighting models[2–5] through an evolution equation for the volume fractions,

$$d\xi^k = \frac{1}{k_p}(\xi_{an}^k - \xi^k)|dH|. \tag{23}$$

Parameter k_p quantifies pinning site density of the material. Pinning refers to material impurities or defects which impede domain wall motion. This hysteresis model, first proposed by Armstrong,[2] employs concepts from the Jiles–Atherton model.[15] In the energy-weighted averaging model frame-

TABLE I. Model parameters.

	$\mu_0 M_s$ (T)	$K_\perp, K_\parallel$ (kJ/m^3)	$(3/2)\lambda_{100}$ ($\times 10^{-6}$)	$3\lambda_{111}$ ($\times 10^{-6}$)	Ω (J/m^3)	k_p (J)	c	E (GPa)
⟨100⟩ $Fe_{81.5}Ga_{18.5}$	1.55	35, 34	255	N/A	1100	230	0.1	75
⟨100⟩ $Fe_{79.1}Ga_{20.9}$	1.21	9.95, 2.0	210	N/A	500	N/A	N/A	N/A
⟨110⟩ $Fe_{81.6}Ga_{18.4}$	1.58	100, 100	290	−40	800	300	0.1	150

work, domain wall motion is indirectly accounted for through changes in the volume fractions. The energies described in Sec. II A pertain to SW particles which approximately represent domain orientations. The anhysteretic volume fractions ξ_{an}^k are calculated through the averaging function [Eq. (2)], which is a function of stress and magnetic field. As stress and magnetic field change, the volume fractions change. Physically, the changes occur through motion of domain walls where this motion causes regions aligned along favorable domain orientations to grow at the expense of the other regions. As the walls pass through defect sites, energy is lost. In the Jiles–Atherton model, which is a domain wall motion model and does not involve volume fractions and domain rotation, this loss is included through a differential equation for magnetization.

The model represented by Eq. (23) has three deficiencies: (1) it does not account for hysteresis when stress is varied at constant field, (2) minor loops exhibit an unphysical, negative differential susceptibility at the reversal points, and (3) it is one-dimensional. Reported Galfenol measurements indicate that hysteresis is more significant for stress application than for field application.[16] In this work, the reason for the apparently wider hysteresis loops for stress application is found to be that for Galfenol, the Zeeman energy [Eq. (5)] is generally larger than the magnetomechanical coupling energy [Eq. (4)].

Since both stress and field change the domain volume fractions through domain wall motion, a single evolution equation should describe the volume fractions in the presence of energy loss from wall pinning for both stress and field application. Additionally, reversible volume fraction changes from domain wall bowing should be accounted for while restricting the irreversible changes predicted by the model which lead to unphysical, negative differential susceptibility. The irreversible changes are described by a modified form of Eq. (23) which includes stress application and consistent scaling

$$d\xi_{irr}^k = \frac{\zeta}{k_p}(\xi_{an}^k - \xi_{irr}^k)[\mu_0 M_s(|dH_1| + |dH_2| + |dH_3|) + (3/2)\lambda_{100}(|dT_1| + |dT_2| + |dT_3|) + 3\lambda_{111}(|dT_4| + |dT_5| + |dT_6|)]. \quad (24)$$

In this extended evolution equation, 3D inputs are included and scaled appropriately so that each input has units of energy density, hence k_p has units of energy density. The value of ζ is zero or one and used to restrict irreversible changes to physically appropriate situations. First the fractional change is calculated with $\zeta=1$ and if the resulting increment gives a negative susceptibility, then it is changed to zero. This condition was given by Jiles *et al.*[17] The total volume fraction change is

$$d\xi^k = (1-c)d\xi_{irr}^k + cd\xi_{an}^k, \quad (25)$$

in which c is nondimensional and has a value between zero and one. For a value of one, volume fraction changes are completely reversible and for a value of zero they are completely irreversible.[18] The magnetic hysteresis model for magnetomechanical materials defined by Eqs. (24) and (25) describes magnetic hysteresis for 3D field and stress inputs. By including reversible magnetization changes and restricting irreversible changes to physically relevant cases, minor loops do not have unphysical negative differential susceptibility as exhibited by the previous model [Eq. (23)]. Figure 6 demonstrates this improvement.

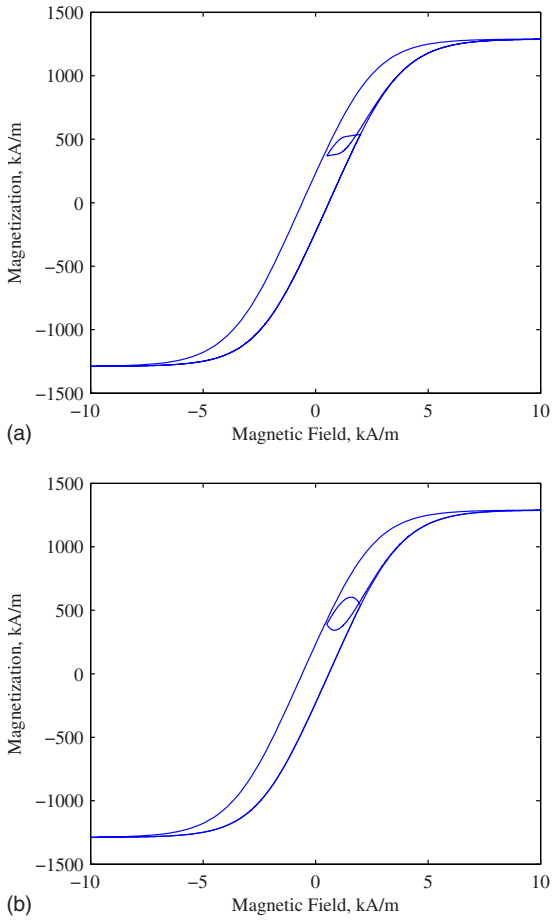

FIG. 6. (Color online) Minor loop calculations using (a) the discrete energy-averaged model and (b) the Armstrong model.

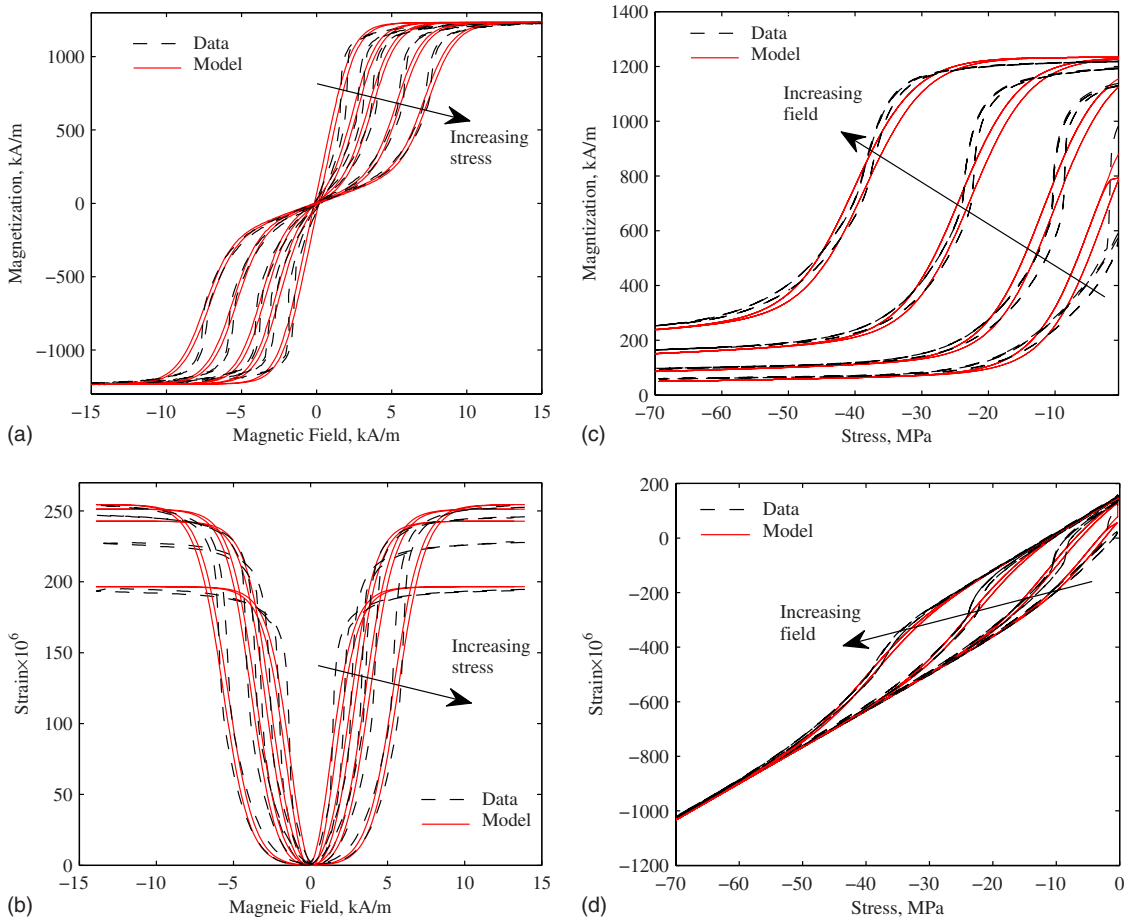

FIG. 7. (Color online) Measurement and model calculations for ⟨100⟩ $Fe_{81.5}Ga_{18.5}$ grown with FSZM at constant stress values of 0.32, 8.00, 13.4, 23.1, and 32.3 MPa (compression) and constant field values of 1.85, 3.24, 5.65, and 8.88 kA/m.

C. Comparison with experiments

1. ⟨100⟩ textured $Fe_{81.5}Ga_{18.5}$ measurements and hysteretic model

Measurements of ⟨100⟩-oriented, textured $Fe_{81.5}Ga_{18.5}$ grown with the Free Stand Zone Melt method (FSZM) at Etrema Products Inc. are compared with model calculations. The magnetostriction measurements (see Fig. 7) indicate a slightly tetragonal magnetic anisotropy but much less so than the higher Ga content sample grown with the Bridgman technique. The ratio of the maximum magnetostriction under zero stress and at 32.3 MPa is 1.34. Increasing the stress beyond 34.3 MPa does not result in high magnetostriction, indicating that the maximum magnetostriction in this case is $(3/2)\lambda_{100}$. The zero stress magnetization versus field curve has a slightly kinked shape. This also suggests that $K_{\perp} > K_{\parallel}$ or that the magnetic anisotropy is tetragonal. The anhysteretic model parameters were determined in the same manner as for the 20.9% Ga sample. The parameters in the hysteresis model k_p and c determine the width of the hysteresis loops and were found through least-squares optimization.

Figure 7 demonstrates the close agreement between model and data. The pinning energy density k_p characterizes the width of the hysteresis loops for both field and stress application. It is the material properties which describe the anhysteretic behavior that account for the apparently wider magnetic hysteresis loops when stress is applied. In the hysteresis model [Eq. (24)], it is the ratio of the applied energy to the pinning energy that determines the hysteresis delay. Since Galfenol alloys have high saturation flux density $\mu_0 M_s$ and moderate maximum magnetostriction $(3/2)\lambda_{100}$, the energy from magnetic field application is higher than the energy from stress application. It is energetically easier to overcome the pinning energy by applying a magnetic field.

Hysteresis is most significant in the burst regions where volume fraction changes occur and negligible where the magnetization process is dominated by domain rotation. For example, in the magnetization versus magnetic field measurement with the highest bias stress (32.3 MPa), there is little hysteresis in the range $-5 < H < 5$ kA/m, where $\xi_{010} + \xi_{0\bar{1}0} + \xi_{001} + \xi_{00\bar{1}} \approx 1$ and magnetization changes are dominated by rotation of domains away from the four perpendicular ⟨100⟩ easy directions and towards the magnetic field. Above 5 kA/m, the ⟨100⟩ easy direction aligned with the field becomes the global minimum which causes a change in the anhysteretic volume fractions [Eq. (2)] which drives the first-order hysteresis model [Eq. (24)]. For field application at constant stress, the first-order [Eq. (24)] has a pseudotime constant $k_p/\mu_0 M_s$ (the coefficient of the field increment) which determines how the volume fractions approach the anhysteretic volume fractions. Thus smaller k_p and larger $\mu_0 M_s$ reduces the field delay associated with hysteresis. Above 10 kA/m, there is no more change in the anhysteretic

volume fractions because $\xi_{[100]} \approx 1$, and as the volume fractions ξ_{irr}^{k} approach this state, there is no more hysteresis.

Consider now the magnetization versus stress curve at the highest bias field (8.88 kA/m). At zero stress, the bias field is enough to align all domains in the [100] direction since its energy is significantly lower than the four perpendicular directions. As the material is loaded in compression, the perpendicular orientations eventually become globally minimum at around 35 MPa. At this point the anhysteretic volume fractions change, which drives the first-order hysteresis model [Eq. (24)]. For stress application at constant field, the first-order [Eq. (24)] has a pseudotime constant $k_p/(3/2)\lambda_{100}$ which determines the stress delay as the volume fractions approach the anhysteretic values. A smaller k_p again reduces the delay as well as a larger λ_{100}. Above 50 MPa, the volume fractions have reached the anhysteretic fractions which are no longer changing, $\xi_{010}+\xi_{0\bar{1}0}+\xi_{001}+\xi_{00\bar{1}} \approx 1$. At this point the magnetization is dominated by domain rotation as the stress competes with the bias field to more fully align domains in the four perpendicular ⟨100⟩ crystal directions. This rotation is described by Eq. (19). The rotation region is linear for applied field because Eq. (19) is linear in H, however for stress application the rotation region is nonlinear since stress appears in the denominator of Eq. (19).

The lower bias field cases (1.85 and 3.24 kA/m) have more complex behavior. The first stress cycle is not a closed loop whereas subsequent cycles are closed for both the measurements and the model calculations. This can be understood with the hysteresis model. The first stress cycle has a different initial condition than subsequent cycles. In collecting the measurements, the material is first saturated with a magnetic field at zero stress followed by a reduction in the magnetic field to the bias field value. At saturation, $\xi_{[100]} = \xi_{an,[100]} = 1$ and when the field is decreased to the bias point, $(\xi_{[100]} > \xi_{an,[100]}) < 1$ since there is a delay in the volume fraction change. This is the starting point of the first stress cycle. During the first cycle, the stress (compressive) is increased until $\xi_{[100]} = \xi_{an,[100]} = 0$ or all the domains are in the perpendicular orientations. Upon reduction in the stress to zero, $\xi_{an,[100]}$ increases, but due to the hysteresis delay, $(\xi_{[100]} < \xi_{an,[100]}) < 1$. Hence the final magnetization is less than the initial magnetization for the first stress cycle since the starting and ending values of the volume fractions are different. Additional stress cycles return to the same volume fraction values and hence subsequent loops are closed.

In the strain versus stress curves, the ΔE effect is observed in both the model and the measurements. The linear regions are governed by Hooke's law and are used to determine Young's modulus E, listed in Table I. The steepest part of the active region, where the effective modulus decreases significantly, is hysteretic since domain volume fractions change in this region. The hysteresis observed in the strain for both applied field and stress is due to the delay in volume fraction changes in magnetic domains, therefore, magnetic hysteresis is responsible for the energy loss in both the magnetization versus field relationship and in the strain versus stress relationship.

2. ⟨110⟩ single-crystal $Fe_{79.1}Ga_{20.9}$ measurements and hysteretic model

For [110] application there are three distinct contributions from the six variants. The variants which dominate the positive saturation region have their easy axes closest to the positive field direction [100] and [010], and rotate until they are aligned parallel to the field (when field is applied at constant stress.) The variants which dominate the negative saturation region have their easy axes closest to the negative field direction $[\bar{1}00]$ and $[0\bar{1}0]$, and rotate until they are aligned parallel to the field. Finally, the variants which dominate the low field region, prior to the burst towards saturation of the magnetization versus field curves, have easy axes perpendicular to the field, [001] and $[00\bar{1}]$. Utilizing Eq. (11), the component of the orientation in the [110] direction for the variants with easy axes perpendicular to the field and stress is

$$m_{\perp} = \frac{\mu_0 M_s}{K_{\perp} - (3/2)(\lambda_{100} + \lambda_{111})T} H. \tag{26}$$

The energy of these directions is

$$E_{\perp} = \frac{(\sqrt{2}\mu_0 M_s H)^2 - 3K_{\perp}(\lambda_{100} + \lambda_{111})T + 2K_{\perp}^2}{6(\lambda_{111} + \lambda_{100})T - 4K_{\perp}}. \tag{27}$$

The component of the orientation in the [110] direction for the variants with easy axes closest to the positive field direction is

$$m_{\parallel +} = \frac{\mu_0 M_s}{2K_{\parallel} - 3\lambda_{100}T} H + \frac{\sqrt{2}}{2}\left(1 + \frac{3\lambda_{111}}{2K_{\parallel} - 3\lambda_{100}T}\right). \tag{28}$$

The energy of these directions is

$$E_{\parallel +} = \frac{(\sqrt{2}\mu_0 M_s H)^2 + 6\sqrt{2}((\lambda_{111} - \lambda_{100})HT + (2/3)K_{100}H)\mu_0 M_s}{12\lambda_{100}T - 8K_{\parallel}} + \frac{9(\lambda_{111}^2 - \lambda_{100}^2)T^2 + 4K_{\parallel}^2}{12\lambda_{100}T - 8K_{\parallel}}. \tag{29}$$

Finally, the component of the orientation in the [110] direction for the variants with easy axes closest to the negative field direction is

$$m_{\parallel -} = \frac{\mu_0 M_s}{2K_{100} - 3\lambda_{100}T} H - \frac{\sqrt{2}}{2}\left(1 + \frac{3\lambda_{111}}{2K_{\parallel} - 3\lambda_{100}T}\right). \tag{30}$$

The energy of these directions is

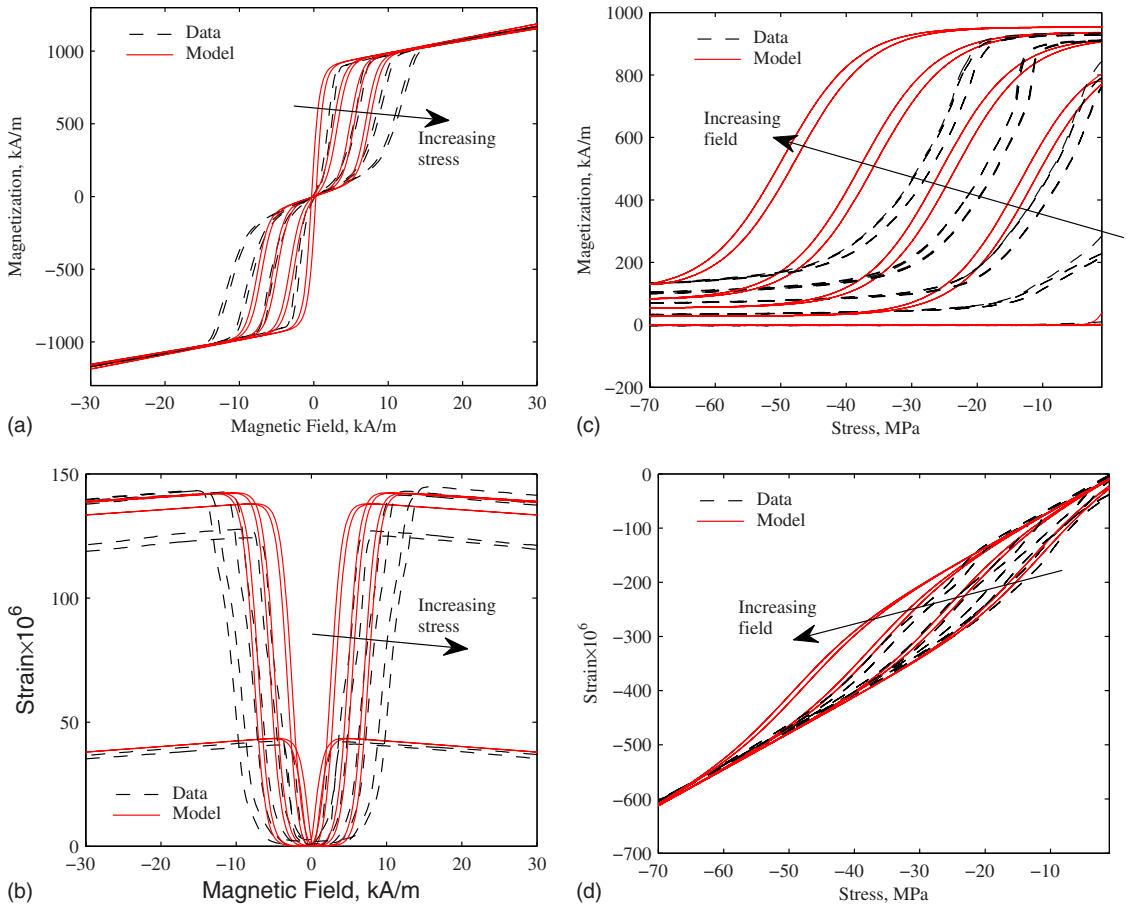

FIG. 8. (Color online) Measurement and model calculations for ⟨110⟩ $Fe_{81.6}Ga_{18.4}$ grown with the Bridgman method at constant stress values of 0.644, 22.1, 39.5, and 55.3 MPa (compression) and constant field values of 0, 1.61, 3.23, 4.84, and 6.46 kA/m.

$$E_{\|-} = \frac{(\sqrt{2}\mu_0 M_s H)^2 - 6\sqrt{2}((\lambda_{111}-\lambda_{100})HT + (2/3)K_{\|}H)\mu_0 M_s}{12\lambda_{100}T - 8K_{\|}} + \frac{9(\lambda_{111}^2-\lambda_{100}^2)T^2 + 4K_{\|}^2}{12\lambda_{100}T - 8K_{\|}}. \tag{31}$$

Since the S–W orientations are calculated with first-order accuracy, the magnetostriction should also have first-order accuracy. Linearization of the particle magnetostriction [Eq. (6)] gives,

$$\mathbf{S}_m \approx \mathbf{S}_{m,0} + \frac{\partial \mathbf{S}_m}{\partial \mathbf{m}}(\mathbf{m}-\mathbf{m}_0). \tag{32}$$

For [110] application with high bias stress, the total magnetostriction (as measured in the [110] direction) at high fields, or above the burst region, is the difference between the magnetostriction of the [100], [010], $[\bar{1}00]$, $[0\bar{1}0]$ easy axis variants and the [001] and $[00\bar{1}]$ easy axis variants. This is because the material starts completely in the latter variants and after the burst region is completely in the former variants. This gives,

$$S_m = \frac{3\sqrt{2}\mu_0 M_s \lambda_{111}}{4K_{\|} - 6\lambda_{100}T}H + \frac{(18\lambda_{111}^2 - 3\lambda_{100}^2)T + 2\lambda_{100}K_{\|}}{8K_{\|} - 12\lambda_{100}T} + \frac{\lambda_{100}}{2}, \tag{33}$$

for the total magnetostriction at high fields. The presence of λ_{111} in the coefficient of H explains how it is possible to have negative piezomagnetism at high fields. The sign depends on the sign of λ_{111}. For the measurements shown in Fig. 8, the slope of the magnetostriction versus magnetic field curve is negative above the burst region. The anhysteretic model properties $K_{\perp}$, $K_{\|}$, $\mu_0 M_s$, λ_{100}, and λ_{111} can all be found by measuring the slopes of the linear regions in the magnetization and magnetostriction versus magnetic field curves and comparing with the analytic expressions [Eqs. (26), (28), and (30)]. The remaining model parameters are found from least-squares optimization.

The analytic expressions accurately describe the data in the domain rotation regions. There is negligible error in the

linear regions below and above the burst regions in the magnetization versus magnetic field curves. Additionally, the correct magnitudes and slopes are predicted by the model for the magnetostriction above and below the burst region, including the negative slope in the magnetostriction at high fields. In both the measured curves and the model curves, the magnetic hysteresis is again more significant for stress application than for magnetic field application. The pseudotime constant for field application is the same as for ⟨100⟩ application, however for the stress it is

$$\tau = \frac{k_p}{(3/2)\lambda_{100} + 3\lambda_{111}}. \tag{34}$$

The negative λ_{111} thus increases the hysteresis delay as compared to ⟨100⟩ application.

There is a discrepancy between the model and the experiments regarding the location of the burst region. The predicted field location is lower and the predicted stress location is higher. The location of the burst region caused by volume fraction changes from the perpendicular variant to the variant with easy axes closer to the field direction is governed by $E_\perp = E_{\parallel +}$ for positive field application and $E_\perp = E_{\parallel -}$ for negative field application. Therefore, the error suggests a missing energy term. However, modification of the energies needs to be done with care since the S–W particle orientations are calculated from the energies and the particle orientations are correctly predicted by the model, as evidenced by the excellent correlation between the model and the measurements in the anhysteretic regions dominated by domain rotation. The details of the burst region are also affected by the energy weighting scheme [Eq. (2)]. Thus, the discrepancy may be a consequence of unmodeled details in the underlying domain wall motion process which causes the volume fraction changes. The same discrepancy is observed when employing the Armstrong model with the global energy definitions since as was demonstrated earlier, both models predict the same location for the burst region [see Fig. 2(b)].

III. CONCLUDING REMARKS

This work extends the energy-weighted averaging class of magnetomechanical models by developing an efficient implementation for magnetic hysteresis due to both applied field and stress. By using local energy formulations dependent on the magnetic easy axes, the formulation is 100 times faster than previous energy weighting models and is applicable to materials with any symmetry of magnetocrystalline anisotropy. Since the hysteresis model accounts for magnetic hysteresis for both field and stress application, it provides a means to understand the history dependence of the magnetization and strain including the apparently larger hysteresis delay for stress application than for field application. Because the model uses analytic expressions for domain rotation, most of the model parameters can be directly determined from features of the measurements. These analytic expressions accurately describe the nonlinear magnetization and strain versus field and stress behavior in regions where domain rotation is the dominant process. In addition to furthering the understanding of Galfenol magnetomechanical behavior, this work provides an efficient modeling framework for Galfenol devices subjected to 3D magnetic field and stress loading, operated in nonlinear and hysteretic regimes.

ACKNOWLEDGMENTS

We wish to acknowledge the financial support by the Office of Naval Research, MURI under Grant No. N000140610530 with program manager Jan Lindberg and the Naval Research Enterprise Internship Program with mentors Marilyn Wun-Fogle and James Restorff.

[1] W. D. Armstrong, J. Appl. Phys. **81**, 2321 (1997).
[2] W. D. Armstrong, J. Magn. Magn. Mater. **263**, 208 (2003).
[3] J. Atulasimha, G. Akhras, and A. B. Flatau, J. Appl. Phys. **103**, 07B336 (2008).
[4] P. G. Evans and M. J. Dapino, IEEE Trans. Magn. **44**, 1711 (2008).
[5] P. G. Evans and M. J. Dapino, J. Appl. Phys. **105**, 113901 (2009).
[6] J. B. Restorff, M. Wun-Fogle, A. E. Clark, and K. B. Hathaway, IEEE Trans. Magn. **42**, 3087 (2006).
[7] C. Kittel, Rev. Mod. Phys. **21**, 541 (1949).
[8] D. C. Jiles and J. B. Thoelke, J. Magn. Magn. Mater. **134**, 143 (1994).
[9] F. Liorzou, B. Phelps, and D. L. Atherton, IEEE Trans. Magn. **36**, 418 (2000).
[10] J. Atulasimha, A. B. Flatau, and E. Summers, Smart Mater. Struct. **16**, 1265 (2007).
[11] S. Chikazumi, *Physics of Magnetism* (Wiley, New York, 1964).
[12] E. D. Trémolet de Lacheisserie, *Magnetostriction* (CRC, Boca Raton, Florida, 1993).
[13] P. G. Evans, PhD Dissertation, Ohio State University, Columbus, Ohio, 2009.
[14] T. A. Lograsso and E. M. Summers, Mater. Sci. Eng., A **416**, 240 (2006).
[15] D. C. Jiles and D. L. Atherton, J. Appl. Phys. **55**, 2115 (1984); http://link.aip.org/link/?JAP/55/2115/1
[16] J. Atulasimha, A. B. Flatau, and R. A. Kellogg, J. Intell. Mater. Syst. Struct. **17**, 97 (2006).
[17] D. C. Jiles, J. B. Thoelke, and M. K. Devine, IEEE Trans. Magn. **28**, 27 (1992).
[18] D. C. Jiles and D. L. Atherton, J. Magn. Magn. Mater. **61**, 48 (1986).